PHYSICAL REVIEW B **69**, 125327 (2004)

Strain distribution in nitride quantum dot multilayers

V. Chamard,[1,*] T Schülli,[2] M. Sztucki,[2] T. H. Metzger,[2] E. Sarigiannidou,[3] J.-L. Rouvière,[3] M. Tolan,[1] C. Adelmann,[3,†] and B. Daudin[3]

[1]*Experimentelle Physik I, Universität Dortmund, Otto Hahn Strasse 4, 44221 Dortmund, Germany*

[2]*European Synchrotron Radiation Facility, BP 220, 38043 Grenoble Cedex, France*

[3]*CEA-CNRS group, "Nanophysique et semiconducteurs," Département de Recherche Fondamentale sur la Matière Condensée, CEA/Grenoble, 17 rue des Martyrs, 38054 Grenoble Cedex 9, France*

(Received 19 August 2003; revised manuscript received 18 December 2003; published 18 March 2004)

Nitride quantum dots (QD's) grown in the wurtzite phase present a strong vertical ordering along the (0001) direction when they are stacked in multilayers. This alignment results from a minimum of the elastic energy density at the surface of the AlN capping layer induced by the buried GaN dot underneath. The aim of this work is to investigate the strain distribution in a quantum dot multilayer using high-resolution transmission electron microscopy and anomalous grazing incidence x-ray diffraction. This x-ray method is based on the strong sensitivity of the elastic scattering cross section to the Ga compounds for energies in the vicinity of the Ga absorption edge. It is observed that uncapped GaN dots are almost completely relaxed, while embedded quantum dots are compressively strained. In addition, a modulation of the in-plane lattice parameter in the AlN spacer layer is clearly identified, induced by the QD's on the surrounding matrix which causes the vertical alignment.

DOI: 10.1103/PhysRevB.69.125327 PACS number(s): 68.55.−a, 68.65.Hb, 68.37.Lp, 61.10.Nz

I. INTRODUCTION

The growth of complex semiconductor heterostructures, such as quantum wells, quantum wires, and quantum dots, has become of great importance aiming for novel optical and electronic properties.[1] A large number of growth procedures involves the epitaxy of lattice mismatched materials using the strain relief as the driving force for the growth of three-dimensional (3D) quantum structures.[2] When grown coherently and stacked in a multilayer, the interacting strain field induced by the quantum dots (QD's) through the thin spacer layer leads to a narrowing of their size and shape distributions. It reaches a minimum after the deposition of the few first bilayers.[3,4] Simultaneously, a vertical order is also obtained, which, depending on the anisotropy of the elastic constants, yields to the formation of 1D to 3D QD crystal lattice.[5,6] Apart from structural and epitaxial growth aspects, the strain fields modify the electronic and optical properties in and around the dots.[7] Several works based on elasticity theory calculations, atomistic simulations, or high-resolution transmission electron microscopy (HRTEM) report on the investigation of the strain distribution of QD multilayers in Si/Ge,[7,8] arsenide[9] and phosphide[10] systems. It is shown that the capping of the QD's clearly modifies the strain field inside the dots while, depending on the thickness of the capping layer, strong deformations of the surrounding matrix are also observed.[7,8,10]

Among the large variety of nanostructured materials, nitride compounds are of particular interest because they show a luminescence in the blue-ultraviolet wavelength range, opening the way to promising applications in optoelectronics. However, the expectations are limited by the large number of dislocations in the material, up to $1-10\times10^{10}\ \mathrm{cm}^{-2}$, which leads to nonradiative recombinations and premature aging of the devices.[11–13] Large efforts are currently under way to reduce the dislocation density by investigating, e.g., different pretreated substrates together with various growth conditions. Another strategy is based on the growth of QD's that could confine the carriers in dislocation free material and limit thereby the nonradiative recombination.[14,15] Most often the growth of the QD's is driven by the Stranski-Krastanov mode[16] during the molecular beam epitaxy of the lattice mismatched GaN on the AlN layer[17] (in-plane lattice mismatch $\Delta a/a=2.4\%$ for the wurtzite phase). They present a truncated pyramidal shape with $\{10\bar{1}3\}$ facets and a hexagonal base with a typical diameter of a few hundreds of angstroms and a typical height to base ratio of 0.2.[14] During growth, the strain state and the dimension (2D or 3D) of the deposited material are monitored by reflection high-energy electron diffraction (RHEED), which indicates before covering that the top of the GaN quantum dots is almost completely elastically relaxed while the bottom is pseudomorphically strained to the wetting layer.[18] For application purposes, it is necessary to bury the QD's in an AlN matrix and to stack them in a multilayer. A strong vertical QD correlation is developing. For this system we have shown that the vertical ordering results from a single well-defined minimum in the elastic energy density distribution at the surface of the capping layer[19] and that the role of threading dislocations in the vertical alignment is certainly faint.[13] The minimum is localized above the previously buried dot due to the isotropy of the elastic constants. A few experimental or theoretical works report on the study of the local strain in this system: they successively address the absence of intermixing between GaN and AlN, the epitaxial relation between the dot and the surrounding matrix, the strains in the buried dot and in the surrounding matrix.[20–22]

The aim of this work is to study the strain distribution directly in a QD multilayer: this investigation results from the use of the unique properties of x-rays of being chemically and strain sensitive; the information given by anoma-

 ©2004 The American Physical Society

lous x-ray diffraction is obtained in a nondestructive way and averaged over a large number of nanostructures.[23] In addition, HRTEM is used to obtain a real-space outlook of the QD shape and size, although the sample preparation is invasive and the number of probed nanostructures is limited. The combination of HRTEM and anomalous x-ray diffraction is thereby a powerful tool to measure and identify unambiguously the strain distribution in the QD multilayer. These techniques, x-ray diffraction and more generally x-ray scattering, have been recently widely used to investigate a large variety of nanostructured semiconductors (for a review on the topic see, e.g., Refs. 24,25) in order to measure the strain, shape, and chemical composition in free-standing[26,27] or buried QD's (Ref. 28), and to quantify the ordering in QD multilayers.[29,19] Most often, the data analysis is based on a comparison of measured and calculated reciprocal space maps using finite element methods based on elasticity theory.[27,28] In a more direct way, strain and composition profiles in free-standing QD's can be obtained using the isostrain scattering method.[26] Recently, anomalous x-ray diffraction has been used for the investigation of free-standing SiGe islands, which does not require *a priori* hypothesis.[30,31] To our knowledge, anomalous x-ray diffraction is used in the present work for the first time on a QD multilayer sample. Due to the large mosaic spread (0.8–1°) in nitride compounds, the complete method described in Ref. 31 cannot be directly applied. However, the use of grazing incidence anomalous x-ray diffraction at the Ga *K* edge allows to investigate the strain in the different regions of the multilayer. Actually, in absence of interdiffusion,[20,22] the presence of gallium is a direct marker of the dots and wetting layers. The combined use of the grazing incidence geometry[32] allows to compare the near surface to the in-depth structure by varying the penetration depth.

The paper is organized as follows: the sample preparation and the experimental setups are detailed in the first part. The second part presents the results and the analysis of real-space investigations using HRTEM. The strain and chemically sensitive investigation of the in-plane lattice mismatch using anomalous grazing incidence x-ray diffraction is described in the third section together with the details of the structural models used for the data analysis. The results are discussed in the last part, where the validity of the structural models, the capping induced strain, the QD induced strain, and the vertical alignment are successively addressed.

II. EXPERIMENTAL DETAILS

The QD GaN/AlN multilayer sample is grown in a commercial MECA 2000 molecular beam epitaxy growth chamber equipped with Ga and Al effusion cells. Active nitrogen is generated by a radio-frequency plasma cell from the EPI company. The substrate consists of a (0001) oriented 5000 Å thick AlN buffer on a bulk 6H-SiC substrate, whose temperature is fixed to 730°C. The 80 bilayers are deposited under N-excess condition with equivalent thicknesses of 100 Å and 15 Å, for AlN and GaN, respectively. With these conditions, the deposition of the about six GaN monolayers leads first to the growth of a two monolayer wetting layer pseudomorphically strained to the AlN. The elastic relaxation of the mismatch-induced strain leads then to the spontaneous formation of the QD's. Each of the QD layers is covered by the AlN spacer layer. A steady state of the QD growth is reached after the deposition of 2–3 bilayers.[13] An uncapped QD layer is grown additionally on the top of the structure in order to measure with atomic force microscopy the dot density which is about 5.5×10^{10} cm^{-2} (Fig. 1).

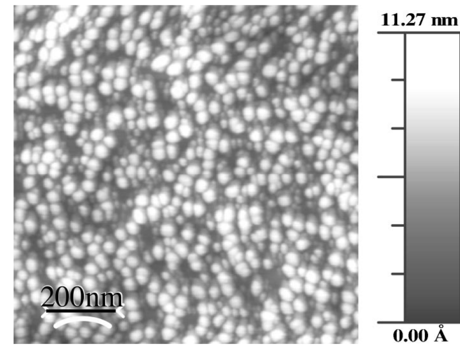

FIG. 1. Atomic force microscopy image of the uncapped QD's at the surface of the QD multilayer sample.

The HRTEM images are performed with a JEOL4000EX electron microscope which has a Scherzer resolution of about 1.7 Å. The preparation of the TEM specimens is made using the standard techniques of mechanical polishing and Argon ion milling.[13]

Due to the small amount of material in the multilayers, a highly brilliant x-ray beam delivered by the third generation synchrotron facilities is mandatory for the x-ray investigations. In this context, the ID1 beamline of the European Synchrotron Radiation Facility in Grenoble (France) is well suited for x-ray diffraction measurements in the grazing incidence geometry combined with the tunability of the beam energy for anomalous scattering. The position in the reciprocal space is described by the wave-vector transfer $\mathbf{q}=\mathbf{k_f}-\mathbf{k_i}$, where $\mathbf{k_i}$ and $\mathbf{k_f}$ are the wave vectors corresponding to the incident and diffracted beams, respectively. In the grazing incidence geometry, the surface is illuminated with a monochromatic beam under a small incidence angle α_i. Because the real part of the refractive index is slightly smaller than unity for x-rays, a regime of total external reflection occurs for α_i smaller than a critical angle α_c. The evanescent wave probes essentially the first 100 Å below the surface. For $\alpha_i>\alpha_c$, the penetration depth increases and the complete multilayer is probed. The diffracted intensity measured around the in-plane $(22\bar{4}0)$ reflection is collected with a linear position sensitive detector oriented vertically with respect to the sample surface. A description of this geometry can be found in Ref. 29.

III. RESULTS AND ANALYSIS

A. High-resolution transmission electron microscopy

The cross-sectional HRTEM image of Fig. 2(a) observed along the $[2,\bar{1},\bar{1},0]$ direction depicts a general view of five GaN QD layers embedded in the AlN matrix. The dots are

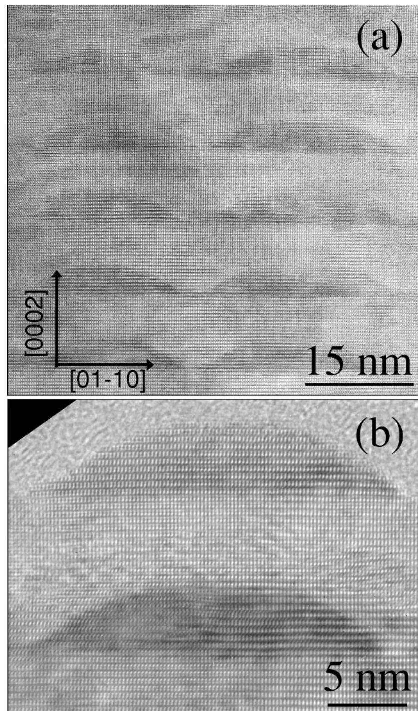

FIG. 2. High-resolution transmission electron microscopy investigation of the QD multilayer sample observed along the $[2,\bar{1},\bar{1},0]$ direction: (a) stack of five QD layers in the multilayer and (b) QD's in the two first top most layers, one uncapped QD at the surface above a capped QD.

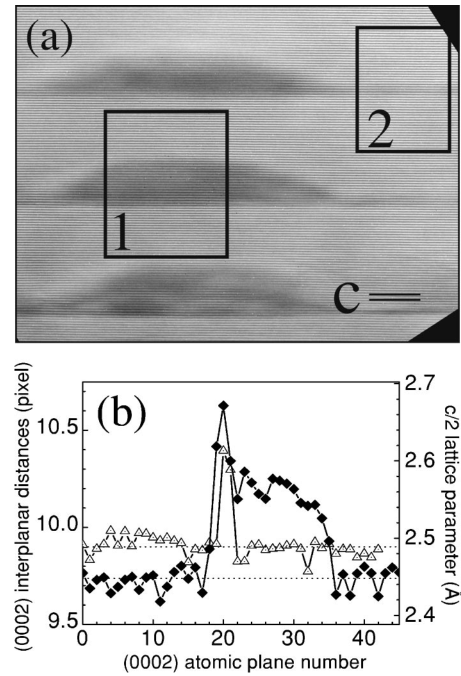

FIG. 3. (a) High-resolution off-axis image of three QD's. Only the (0002) planes are visible. The interplanar distance used to scale the *c* axis is shown at the right bottom corner. (b) Lattice fringe profiles in pixel units and in angstrom measured through the regions 1 (full dots) and 2 (open dots) defined in (a) (the solid line is only a guide for the eye). The horizontal dotted lines represent the average values in the AlN matrix.

vertically aligned and well separated from each other. The wetting layer aside the QD's is also visible. The Fig. 2(b) shows the QD's in the first two topmost bilayers: one uncapped QD at the surface above a capped QD. The shape and size of the capped QD's are very similar to the uncapped ones. By analyzing HRTEM images of different directions in combination with the atomic force microscopy measurements, the dots are found to present a truncated pyramidal shape with walls inclined by $30°$ from the surface plane, corresponding to the usual $\{10\bar{1}3\}$ facets. The average height and base diameter are about 40 Å and 300 Å, respectively.

Using a projection method[20] together with the geometrical phase method[33] several high-resolution images such as the one presented in Fig. 3(a) are analyzed: the HRTEM image is first projected along the (0002) planes in order to reduce the noise, resulting in an average intensity profile. On this profile, the positions of the intensity maxima are determined by fitting the neighborhood extrema with a polynomial function of second degree. It gives the distances between the successive (0002) planes, which are described as a function of the plane numbers. Two typical lattice fringe profiles extracted from region 1 through the QD (full dots) and from region 2 through the wetting layer (open dots) are shown in Fig. 3(b). In the profile 2, the thickness of the wetting layer is estimated to about 2–3 monolayers[20] and the layer presents a Ga polarity.[34] The average values of the interplanar distance along the *c* axis in the AlN matrix are also indicated as dotted lines. They clearly show a lattice mismatch $\Delta c/c$ of about $1.3\pm0.5\%$ (mean-value averaged over the profile series) for the AlN located between two vertically stacked QD's with respect to the AlN located between two consecutive wetting layers. In the case of Ga interdiffusion in the AlN matrix at the top of the QD's, a lattice parameter larger than the lattice parameter in the AlN matrix located between two wetting layers is expected. Our observations show the opposite results which confirms that the interdiffusion is negligible. By assuming that the AlN located between two consecutive wetting layers [profile 2 of Fig. 3(b)] is fully relaxed ($c/2=2.49$ Å), this 1.3% lattice mismatch is understood in the framework of elasticity theory as the stressor action of the relaxed GaN QD's which almost completely strain the AlN located between the QD's.

B. Anomalous grazing incidence x-ray diffraction

1. Measurements

Anomalous grazing incidence x-ray diffraction measurements with beam energy tuned to the Ga *K* edge ($E_{Ga}=10.367$ keV) are performed in order to investigate the strain in the different parts of the QD multilayer together with the Ga content, using the chemical sensitivity of the scattered intensity. In the vicinity of the Ga *K* edge, the Ga atomic scattering factor decreases by a large amount, resulting in a weaker scattered signal for all Ga compounds. In order to measure accurately the Ga *K* edge (which may vary with the energy resolution of the setup and with the Ga crystallographic surrounding), a fluorescence spectra in the clas-

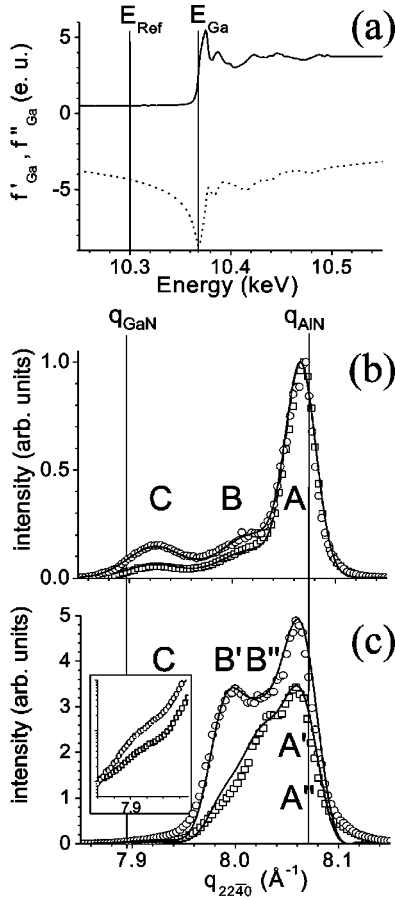

FIG. 4. (a) Anomalous corrections f' (dotted line) and f'' (solid line) for Ga in the vicinity of the *K*-absorption edge. f'' is measured by fluorescence and f' is deduced by the Kramers-Kronig algorithm. The two vertical lines indicate the reference energy ($E_{ref}=10.3$ keV) and the Ga *K* edge ($E_{\mathrm{Ga}}=10.367$ keV). Grazing incidence anomalous x-ray diffraction measurements at the in-plane $(22\bar{4}0)$ reflection along the $q_{\langle 22\bar{4}0\rangle}$ radial direction. The measurements at E_{ref} are given by open circles, while the squares represent the measurements at E_{Ga} for (b) $\alpha_i=0.07°$ and (c) $\alpha_i=0.25°$. The solid lines in (b) and (c) are the results of the best fits using the same model as described in the text. The inset in (c) is a lin-log plot of the region *C*.

sical large angle geometry is first measured with the sample [Fig. 4(a), solid line]. The experimental Ga *K* edge is found at the expected energy within an absolute accuracy of less than 1 eV. A series of diffraction curves in the grazing incidence geometry is then measured at the in-plane $(22\bar{4}0)$ reflection for the two energies marked by a vertical line on the Fig. 4(a): the reference curve (open circles) is measured 67 eV below the Ga K edge ($E_{Ref}=10.3$ keV) and the second one, the anomalous curve, (open squares) directly at E_{Ga} [Figs. 4(b) and 4(c)]. In order to improve the statistics and to avoid the contribution of the multilayer periodicity (for $\alpha_i>\alpha_c$), the α_f spectra are integrated along the linear detector between α_c and $2.4\times\alpha_c$. The relaxed $q_{22\bar{4}0}$ values for GaN and AlN are indicated on the graph as q_{GaN} and q_{AlN}, respectively.

The first series presented in Fig. 4(b) is obtained for an angle of incidence $\alpha_i=0.07°$, much smaller than α_c (measured at about 0.22° for E_{Ref} and E_{Ga}). For this incidence angle, the penetration depth is about 100 Å for the two energies. Both reference and anomalous measurements present an intense diffraction peak, denoted *A*, located around q_{AlN}. On the low $q_{22\bar{4}0}$ range but for $q_{22\bar{4}0}>q_{\mathrm{GaN}}$, a weak double peak intensity is observed on the reference curve (denoted *B* and *C*). On the anomalous measurement, this part is strongly reduced, indicating the presence of Ga. The second series presented on Fig. 4(c) is measured for $\alpha_i=0.25°$. For such a large incident angle, a large number of bilayers is probed as the penetration depth is increased to about 0.5–1 μm. However, in the $\alpha_i>\alpha_c$ region, the penetration depth depends strongly on the energy. Therefore the exact number of probed bilayers is difficult to evaluate. The intense peak located near q_{AlN} remains on the reference curve together with another strong peak located at 8 Å^{-1}. A weak shoulder is also visible around 7.92 Å^{-1}. In the anomalous measurement, a strong modification of the intensity distribution is observed with an important decrease of about all intensity components except in the $q_{22\bar{4}0}\approx 8.03$ Å^{-1} region.

2. Structural model

In the distorted wave Born approximation, the scattered intensity $I(\mathbf{q})$ is given by

$$I(\mathbf{q})\propto T(\alpha_i)|S(\mathbf{q})|^2T(\alpha_f), \tag{1}$$

where $T(\alpha_{i,f})$ are the transmission functions for the incident and exit angle, respectively, and $S(\mathbf{q})$ is the structure factor.[32] In the vicinity of the Ga *K* edge, all terms are very sensitive to the energy. The transmission function can be calculated, using the Parratt formalism[35] for a layered electron density averaged in each sublayer of the multilayer (i.e., wetting layers, QD layers and spacer layers). This approach shows that in the grazing incidence regime $\alpha_i\ll\alpha_c$, the transmission function is rather insensitive to the change of dispersion and absorption, whereas for $\alpha_i\gg\alpha_c$, a strong dependence of the transmission function with both α_i and the complex refractive index profile is observed. Following the same arguments, the penetration depth is almost unchanged for $\alpha_i\ll\alpha_c$ (about 100 Å, i. e., the two topmost bilayers) whereas it changes strongly for $\alpha_i\gg\alpha_c$: for $\alpha_i=0.25°\pm0.01°$, the penetration depth decreases from about 60 ± 10 bilayers down to 25 ± 5 when the energy increases from E_{ref} to E_{Ga}. In addition, small variations in the profile of the complex refractive index also induce strong variations in the penetration depth for $\alpha_i\gg\alpha_c$. Moreover, the AlN buffer layer may also contribute to the diffracted signal, resulting in an unknown offset around q_{AlN}, but only for the E_{Ref} measurement. For these reasons, the $\alpha_i=0.25°$ measurements are only used to validate our structural model resulting from the fit of the $\alpha_i=0.07°$ data, described in the following part.

The structure factor $S(\mathbf{q})$ of a finite-size crystal is given by

$$S(\mathbf{q})=f(q)(\Omega(\mathbf{q})*\Delta(\mathbf{q})), \tag{2}$$

where $f(q)$ is the complex scattering factor of the crystal, $\Omega(\mathbf{q})$ is the Fourier transform of the crystal shape, $\Delta(\mathbf{q})$ represents the strain distribution in the reciprocal space as-

TABLE I. Structural parameters of the three zones A, B, C used to fit the measurements of the Fig. 4(b) and presented on Fig. 5: crystal shape with its corresponding base diameter and height, the in-plane lattice misfit $\varepsilon_{\parallel}=\Delta a/a_{AlN}$, the corresponding strain distribution and the chemical composition of each zone.

Zone	Shape	Diameter (Å)	Height (Å)	$\varepsilon_{\parallel}$ (%)	Strain distribution (%)	Composition (%)
A	Cylinder	220	100	0.06 ± 0.02	22	100% AlN
B	Cylinder	190	100	0.64 ± 0.06	65	60% AlN + 40% GaN
C	Truncated cone	300	40	1.85 ± 0.05	55	100% GaN

sociated with the crystal and * denotes the convolution of the two quantities. As nitride compounds are disturbed materials with defects and as the typical sizes of the structure are rather small, the calculation of the intensity diffracted by the QD multilayer is performed in the incoherent way.[23] In the following, the strain is given as the in-plane lattice parameter misfit $\varepsilon_{\parallel}=\Delta a/a_{\rm AlN}$ ($a_{\rm AlN}=3.114$ Å) between the considered crystal and the relaxed AlN taken as a reference.

At the $(22\bar{4}0)$ reflection of a XN wurtzite compound (X =Al, Ga), the scattering factor is given by

$$f_{X\rm N}(q)=2(f_X(q)+f_{\rm N}(q)), \tag{3}$$

where $f_{X,\rm N}(q)=f_0(q)+f'(E)+if''(E)$ is the complex atomic scattering factor. f_0 represents the q dependence of the Fourier transform of the atomic electron distribution, calculated for Al, Ga, and N with a code derived from Ref. 36; f' and f'' are the real and imaginary parts of the energy (E) dependent corrections that become important, for Ga compounds in the vicinity of the Ga K edge. For a precise determination of the atomic scattering factor of Ga in sample A, $f''_{\rm Ga}$ is deduced from the fluorescence measurement [Fig. 4(a), solid line] and $f'_{\rm Ga}$ is calculated using the Kramers-Kronig dispersion relation for the measured $f''_{\rm Ga}$ values in the vicinity of the edge and tabulated values from Ref. 37 for the remaining part of the spectrum [Fig. 4(a), dotted line].

For the $\alpha_i=0.07°$ measurements [Fig. 4(b)], where only the two topmost bilayers are probed, three peaks are observed. The peak A is located around $q_{\rm AlN}$ and its contribution is weakly affected by the variation of the energy. It is attributed to the relaxed matrix of pure AlN located between two wetting layers (named zone A). The shape of this zone is approximated simply by a cylinder with a diameter corresponding to the interdot distance (about 200 Å, deduced from the QD density) and a height of about 100 Å, corresponding to the penetration depth. This finite-size crystal leads to a diffraction peak width of only 0.03 Å^{-1}, smaller than the experimental one. In order to reproduce the broadening of this Bragg component, it is necessary to introduce a distribution, which exists probably in both size and strain. However, the studies of the single-layer growth mode show that the AlN deposited on a GaN substrate presents a strong in-plane lattice variation during the deposition of the first 50 Å.[38] Similar lattice distribution is observed during the growth of AlN on GaN QD's.[18] Therefore, a simple approximation is done with the use of a normalized Gaussian-like strain distribution of about 20% in order to match the measured broadening of the corresponding peak. The integrated intensity of this Bragg peak is finally well reproduced for a refined diameter of 220 Å. On the other side of the diffraction curves, the weak peak denoted C is attributed to the free-standing QD's on the surface as a chemical composition of 100% GaN is necessary to reproduce the anomalous effect and as the corresponding lattice parameter is closer to relaxed GaN than relaxed AlN. The shape is approximated by a truncated cone with a base diameter of 300 Å, a height of 40 Å (according to our HRTEM results) and an in-plane lattice misfit $\varepsilon_{\parallel}$ of about 1.85%. Between these two extreme peaks, the peak B was first attributed to a strained AlN column under the free-standing QD's. This simple model cannot explain the change of the scattering and therefore this description is rejected. A significant contribution of GaN is needed to explain the intensity decrease at $E_{\rm Ga}$. Finally, this strain state is attributed to a cylindrical zone B which contains the AlN matrix *and* the first buried QD's. The height of the zone B is limited by the penetration depth. From the fit, the diameter of this zone is estimated to about 190 Å, slightly larger than the QD apex diameter (140 Å). Although the exact contribution of GaN is difficult to measure, the estimated amount of GaN is in agreement with the volume ratio of GaN compared to AlN in such a defined cylinder. The $\varepsilon_{\parallel}$ value of the zone B is about 0.65%. The parameters used to fit the measurements of Fig. 4(b) are summarized in Table I and a schematic view of the three zones is represented in Fig. 5(a).

The measurements presented in Fig. 4(c) are obtained for $\alpha_i=0.25°$ where a larger number of bilayers is probed. On the reference curve, the AlN peak is well visible, as well as the peak corresponding to the strained AlN + GaN column, at about 7.98 Å^{-1}. In the small $q_{22\bar{4}0}$ range, the weak scattering from the free-standing QD's at the surface is also distinguishable (see inset). On the measurements performed at $E_{\rm Ga}$, the intensity of the relaxed AlN peak decreases. It results from two parallel effects: (i) the contribution of the AlN buffer which disappears at $E_{\rm Ga}$ due to the decrease of the penetration depth, from about 60 down to 25 bilayers and (ii) the anomalous effects from the GaN wetting layer which is strained to the AlN spacer layer (this second effect is not obvious in the $\alpha_i<\alpha_c$ measurements probably due to intensity normalization uncertainties). At low $q_{22\bar{4}0}$, the weak scattering signal from the free-standing QD's is no more visible, as expected. Finally, the peak in the central part of the diffraction curve decreases tremendously, while the plateau around 8.03 Å^{-1} is almost unchanged. It shows that the ver-

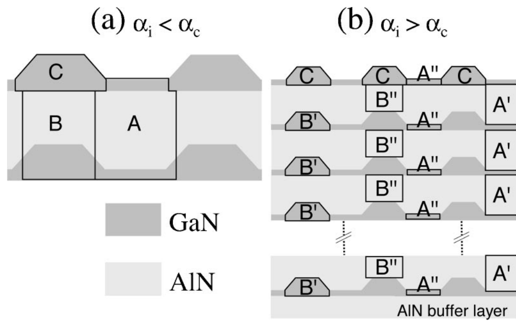

FIG. 5. Schematic views of the structural models used to fit the anomalous grazing incidence diffraction measurements at (a) $\alpha_i < \alpha_c$ [Fig. 4(b)] and at (b) $\alpha_i > \alpha_c$ [Fig. 4(c)]. The dark and light parts represent the GaN and AlN compounds, respectively. The zones labeled on the draws indicate the isostrain regions, as described in the text: (a) between two wetting layers (A), in the first embedded dot layer and the corresponding above AlN matrix (B) and in the free standing quantum dots (C), (b) in the AlN between two wetting layers (A'), in the wetting layers (A''), in the embedded GaN dots (B'), in the corresponding above AlN matrix (B'') and in the free standing quantum dots (C). The same definition also refers to the peaks of Figs. 4(b) and 4(c).

tically aligned QD's present an in-plane lattice misfit slightly larger than the strained AlN matrix in between.

As the structural model needed to understand the measurements requires a large number of parameters, we base our calculations on the same structural parameter values as found for the $\alpha_i < \alpha_c$ measurements and introduce the following five contributions, schematically drawn in Fig. 5(b): the free standing GaN QD's (region C), the embedded QD's (family of regions B'), the AlN matrix between the QD's (family of regions B''), the relaxed AlN matrix (family of regions A'), and the GaN wetting layer (family of regions A''). The decrease of the penetration depth and the buffer layer contribution are also introduced in the calculations. The measurements of Fig. 4(c) can be well reproduced when the strained AlN matrix and the capped QD misfits are set to 0.55% and 1.02%, respectively.

IV. DISCUSSION

The present work studies the strain distribution in a GaN/AlN QD multilayer. The QD growth is driven by the Stranski-Krastanov mode which leads to the formation of 3D islands by elastically relaxing the mismatch-induced strain. When embedded in an AlN matrix and stacked in the multilayer, the QD's show a strong vertical ordering evidenced by HRTEM methods[14,13] and quantified by x-ray scattering techniques.[19] The strain distribution which is responsible for the ordering in several QD multilayer systems is investigated here using both real-space and reciprocal-space approaches. We observed that the free-standing GaN QD's on the surface are slightly strained ($\varepsilon_{\parallel} = 1.85\%$), while they show a more pronounced compressive strain of about 1.02% when they are capped in the AlN matrix. Moreover, a tensile strain of about 0.55% is clearly identified in the AlN spacer layer, which is attributed to the matrix located between two vertically stacked QD's.

Strain distribution studies in GaN/AlN QD multilayer are already addressed in several experimental and theoretical works as the understanding or the prediction of optical and electronic properties motivates the knowledge of the structural properties.[20–22] Moreover, a clear understanding of the growth mechanisms relies on the strain and chemical distribution descriptions. The use of anomalous grazing incidence x-ray diffraction at the Ga K edge gives the unique opportunity to study the strain distribution as a function of the chemical composition in this nitride QD multilayer. The first question arising concerns the validity of our structural model. The main assumption of this work is the absence of interdiffusion: in this case the presence of Ga is a direct signature of the GaN QD's or wetting layers. Thereby, the strain in the different parts of the multilayer can be unambiguously identified. The absence of Al/Ga interdiffusion is in agreement with HRTEM analysis based on the comparison of experimental and simulated HRTEM lattice fringe profiles using linear elasticity theory: rather abrupt interfaces are found.[20] The same conclusion is drawn in Ref. 22 where nonresonant Raman scattering measurements of a GaN/AlN QD multilayer is compared to a thick $Ga_xAl_{1-x}N$ layer of the same average composition. Furthermore, our x-ray simulations are based on a simple model without taking into account the decay of the electromagnetic field in the multilayer. This effect is only of importance for $\alpha_i \geqslant \alpha_c$, where a large number of bilayers, which may present a gradient of structural properties, contributes to the scattered intensity with different weights related to their position in the multilayer. However for a 80 bilayer sample, we may assume that the top 60 bilayers are self-replicated, as the steady state of growth is already reached after the deposition of a few bilayers.[13]

A first main conclusion of this work concerns the measurement of the average strains in the QD's. Let us point out however that no strain profile can be measured with this x-ray method for the GaN/AlN QD's system as the QD size distribution and the strain distribution lead to the same broadening of the x-ray diffraction peaks. The mosaic spread of the deposited nitride compounds avoids any determination of the lateral size and size distribution, usually obtained in rocking scans.[31] Concerning the free-standing QD's at the surface, a slight compressive strain of about 1.85% is obtained instead of the 2.4% lattice mismatch calculated between the bulk GaN and AlN in-plane lattice parameters. This result can be compared to RHEED measurements performed *in situ* during growth, where an almost completely relaxed GaN is monitored on the top of the growing QD's.[18] Moreover, for embedded QD's, a modification of the in-plane misfit is observed enhanced by the comparison with the free-standing QD's. Although the shape is not modified by the capping, the AlN acts as a stressor on the QD's resulting in an in-plane compression in GaN of about 1%. This effect is understood[7,8] and observed for several QD's systems.[10,28] For the GaN/AlN QD system, analytical calculations of the strain tensor in embedded GaN QD's lead to a strain of about 0.3–0.7 %, close to our observation.[21] Some differences in the structural parameters such as the spacer

layer thickness and the QD size may explain this slight discrepancy.[7,8,10] However, our x-ray results differ from our HRTEM analysis: the $\Delta c/c$ lattice mismatch for AlN located between two QD's and AlN located between two wetting layers corresponds to the stressor action of the fully relaxed GaN QD's on the surrounding matrix. In the HRTEM study the thin-specimen relaxation due to the reduce thickness of the TEM samples is not taken into account and explains this difference.[39] Further works are needed to fully quantify this effect, using finite element methods applied on QD thin samples.

Finally, the more important aspect of our study concerns the modulation of the in-plane strain in the AlN spacer layer, which can be observed with x-ray diffraction techniques only by using the chemical sensitivity of the anomalous scattering. While AlN between two wetting layers is almost fully relaxed, the AlN matrix between two vertically stacked QD's is strained to about 0.55%. In comparison, a strain of 0.86% is reported in an indirect way in Ref. 22 assuming some averaging in the complete AlN spacer layer, while a value of 0.4% is calculated in Ref. 21. This local strain results from the stressor action of the QD's on the surrounding matrix and leads to the QD vertical alignment:[3,4] the elastic energy density at the surface of the AlN capping layer presents a well-defined minimum located above the buried QD.[19] The strained area is of the order of the QD base and apex diameters. It is interesting to note that the QD and the surrounding matrix do not present the same average strain in the *a* direction and that none of them is fully relaxed. This information can be used for prediction of carrier confinement properties observed in GaN/AlN QD structures.[14]

V. CONCLUSION

In conclusion, using anomalous x-ray diffraction in the grazing incidence geometry in combination with HRTEM, we investigate the strain distribution in the different parts of the nitride QD multilayer: we observe the capping induced strain on the QD's as well as the in-plane lattice parameter modulation in the spacer layer, which causes the vertical alignment of the dots. This work shows that the anomalous x-ray diffraction techniques can be applied to investigate complex nanostructured multilayers, such as QD multilayers. It opens the way to further investigations of the dependency of the in-plane strain modulation with the spacer layer thickness and with the material elastic constants.

*Corresponding author. Present address: LTPCM, 1130 rue de la piscine, 38402 Saint Martin d'Hères, France. Email address: virginie.chamard@ltpcm.inpg.fr

†Present address: Department of Chemical Engineering and Materials Science, University of Minnesota, 151 Amundson Hall, Box 203, 421 Washington Ave. SE, Minneapolis, MN 55455.

[1] D. Bimberg, M. Grundmann, and N. N. Ledentsov, *Quantum Dots Heterostructures* (Wiley, Chichester, 1999).

[2] V.A. Shchukin and D. Bimberg, Rev. Mod. Phys. **71**, 1125 (1999).

[3] Q. Xie, A. Madhukar, P. Chen, and N.P. Kobayashi, Phys. Rev. Lett. **75**, 2542 (1995).

[4] F. Liu, S.E. Davenport, H.M. Evans, and M.G. Lagally, Phys. Rev. Lett. **82**, 2528 (1999).

[5] V.A. Shchukin, D. Bimberg, V.G. Malyshkin, and N.N. Ledentsov, Phys. Rev. B **57**, 12 262 (1998).

[6] V. Holý, G. Springholz, M. Pinczolits, and G. Bauer, Phys. Rev. Lett. **83**, 356 (1999).

[7] O.G. Schmidt, K. Eberl, and Y. Rau, Phys. Rev. B **62**, 16715 (2000).

[8] M.A. Makeev and A. Madhukar, Phys. Rev. Lett. **86**, 5542 (2001).

[9] T. Benabbas, Y. Androussi, and A. Lefebvre, J. Appl. Phys. **86**, 1945 (1999).

[10] N.Y. Jin-Phillipp and F. Phillipp, J. Appl. Phys. **88**, 710 (2000).

[11] S.D. Lester, F.A. Ponce, M.G. Craford, and D.A. Steigerwald, Appl. Phys. Lett. **66**, 1249 (1995).

[12] E.D. Bourret-Courchesne, S. Kellermann, K.M. Yu, M. Benamara, Z. Liliental-Weber, J. Washburn, S.J.C. Irvine, and A. Stafford, Appl. Phys. Lett. **77**, 3562 (2000).

[13] J.-L. Rouvière, J. Simon, N.T. Pelekanos, B. Daudin, and G. Feuillet, Appl. Phys. Lett. **75**, 2632 (1999).

[14] F. Widmann, B. Daudin, G. Feuillet, Y. Samson, J.-L. Rouvière, and N.T. Pelekanos, J. Appl. Phys. **83**, 7618 (1998).

[15] J. Simon, N.T. Pelekanos, C. Adelmann, E. Martinez-Guerrero, R. André, B. Daudin, Le Si Dang, and H. Mariette, Phys. Rev. B **68**, 035312 (2003).

[16] I.N. Stranski and V.L. Krastanov, Akad. Wiss. Lit. Mainz Abh. Math. Naturwiss. Kl. **146**, 797 (1939).

[17] B. Daudin, F. Widmann, G. Feuillet, Y. Samson, M. Arlery, and J.-L. Rouvière, Phys. Rev. B **56**, R7069 (1997).

[18] C. Adelmann, Ph.D. thesis, Université Joseph Fourier–Grenoble 1 2002.

[19] V. Chamard, T.H. Metzger, M. Sztucki, V. Holý, M. Tolan, E. Bellet-Amalric, C. Adelmann, B. Daudin, and H. Mariette, Europhys. Lett. **63**, 268 (2003).

[20] M. Arlery, J.-L. Rouvière, F. Widmann, B. Daudin, G. Feuillet, and H. Mariette, Appl. Phys. Lett. **74**, 3287 (1999).

[21] A.D. Andreev and E.P. O'Reilly, Phys. Rev. B **62**, 15851 (2000).

[22] J. Gleize, J. Frandon, F. Demangeot, M.A. Renucci, C. Adelmann, B. Daudin, G. Feuillet, B. Damilano, N. Grandjean, and J. Massies, Appl. Phys. Lett. **77**, 2174 (2000).

[23] V. Holý, U. Pietsch, and T. Baumbach, *High Resolution X-ray Scattering From Thin Films and Multilayers*, Springer Tracts in Modern Physics, Vol. 149 (Springer Verlag, Berlin, 1999).

[24] J. Stangl, A. Hesse, T. Roch, V. Holý, G. Bauer, T. Schülli, and T.H. Metzger, Nucl. Instrum. Methods Phys. Res. B **200**, 11 (2003).

[25] M. Schmidbauer, M. Hanke, and R. Köhler, Cryst. Res. Technol. **37**, 1 (2002).

[26] I. Kegel, T.H. Metzger, A. Lorke, J. Peisl, J. Stangl, G. Bauer, K. Nordlund, W.V. Schoenfeld, and P.M. Petroff, Phys. Rev. B **63**, 035318 (2001).

[27] M. Schmidbauer, F. Atami, M. Hanke, P. Schäfer, K. Braune, W.T. Masselink, and R. Köhler, Phys. Rev. B **65**, 125320 (2003).

[28] A. Hesse, J. Stangl, V. Holý, T. Roch, G. Bauer, O.G. Schmidt, U. Denker, and B. Struth, Phys. Rev. B **66**, 085321 (2002).

[29] I. Kegel, T.H. Metzger, J. Peisl, J. Stangl, G. Bauer, and D. Smilgies, Phys. Rev. B **60**, 2516 (1999).

[30] R. Magalhaes-Paniago, G. Meideros-Ribeiro, A. Malachias, S. Kycia, T. I Kamins, and R. Stan Williams, Phys. Rev. B **66**, 245312 (2002).
[31] T.U. Schülli, J. Stangl, Z. Zhong, R.T. Lechner, M. Sztucki, T.H. Metzger, and G. Bauer, Phys. Rev. Lett. **90**, 066105 (2003).
[32] H. Dosch, *Critical Phenomena at Surfaces and Interfaces: Evanescent X-ray and Neutrons Scattering*, Vol. 126, Springer Tracts in Modern Physics (Springer-Verlag, Berlin, 1992).
[33] M.J. Hÿtch, E. Snoeck, and R. Kilaas, Ultramicroscopy **74**, 131 (1998).
[34] E. Sarigiannidou, J.-L. Rouvière, G. Radtke, P. Bayle-Guillemaud, E. Monroy, and B. Daudin, Ins. Phys. Conf. Ser. (to be published).
[35] M. Tolan, *X-ray Scattering from Soft-matter Thin Films,* Vol. 148, Springer Tracts in Modern Physics (Springer-Verlag, Berlin, 1999).
[36] J. Baró, M. Roteta, J.M. Fernández-Varea, and F. Salvat, Radiat. Phys. Chem. **44**, 531 (1994).
[37] L. Kissel, B. Zhou, S.C. Roy, S.K. Sen-Gupta, and R.H. Pratt, Acta Crystallogr., Sect. A: Found. Crystallogr. **51**, 271 (1995).
[38] A. Bourret, C. Adelmann, B. Daudin, J.-L. Rouvière, G. Feuillet, and G. Mula, Phys. Rev. B **63**, 245307 (2001).
[39] K. Tillmann and W. Jäger, J. Electron Microsc. **49**, 245 (2000).